International Journal of Thermofluids 24 (2024) 100992

Contents lists available at ScienceDirect

International Journal of Thermofluids

journal homepage: www.sciencedirect.com/journal/international-journal-of-thermofluids

CFD Simulation of the slipper dynamics during variable displacement operations in a swash-plate type axial piston pump

G. Muzzioli , F. Orlandi , M. Venturelli , M. Milani , L. Montorsi

Department of Science and Methods for Engineering, University of Modena and Reggio Emilia, Reggio Emilia, Italy

ARTICLE INFO

Keywords:
Axial piston pump
Slipper
CFD
Variable displacement
Fluid body interaction

ABSTRACT

This paper investigates the effects of the displacement variation in swash plate type axial piston pumps on the dynamics of a vented grooved slipper. A previously validated methodology based on the combined Dynamic Fluid Body Interaction (DFBI) and morphing approach is exploited to continuously update the position of the slipper with respect to the swash plate. The separate contributions of both slipper tilting and axial translation to the instantaneous clearance height are presented, and their consequences on the pressure distribution within the gap are pointed out. Moreover, the pressure induced hydraulic lift on the slipper surfaces is monitored, and a specific balance coefficient is introduced.. The impact of the slipper-swash plate interface on the volumetric efficiency of the pump is quantified by means of local measures of the leakage flow through the coupling clearance. Finally, a detailed comparison of the results at different pumps displacements highlights the most critical conditions.

1. Introduction

Axial piston pumps represent a frequent choice in industry to produce high power density. These machines have been deeply investigated over the last decades and huge improvements have been achieved in terms of both volumetric and mechanical efficiencies. The variable displacement characteristic along with the wide range of working pressure, i.e., up to 400 bar, represent the main merits for axial piston pumps, making them the best choice for load-sensing applications. However, the significant number of internal parts still represent an important demerit of such architecture, where fine couplings are needed to reach the best trade-off between friction and flow losses or, in other terms, to ensure optimal performances.In this paper, the transient evolution of the slipper-swash plate interface in axial piston pumps and motors is investigated by means of the CFD numerical approach under actual operating conditions. Many recent works are found in literature about the optimization of the slipper mechanical and fluid dynamic features in order to improve the overall pump efficiency. In [1], a mathematical definition of the optimal clearance height is presented as a function of several geometrical and operating parameters. However, the constant gap assumption has been considered in the analysis, which is not representative for a real scenario. Indeed, secondary tilting motions apply to the slippers while sliding on the flat surface of the swash plate as a result of the external forces and moments. The consequence for that is a variable clearance height between the parts which deeply affects the pressure distribution and the hydrodynamic lift force. Therefore, a detailed analysis of the slipper dynamics is necessary to fully characterize the interface with the swash plate. Significant progress have been done over the last few years in this sense, not only improving the volumetric and mechanical efficiency of the pumps, but also preventing an excessive wear of the components. In [2], an analytical model for the computation of the power losses in slipper-swash plate interfaces including slipper deformation highlights a major influence of the rotational velocity on the power losses than the external operating pressure. Moreover, a similar approach to [1] for the definition of the optimal gap height in terms of minimum power losses is reported in [3] considering different slipper designs. The importance of a non-flat running surface for a successful slipper operation is pointed out in [4], where a validated test rig for the analysis of the slipper behavior under steady-state conditions is further presented. However, as it is stated by the same authors, many difficulties must be faced to experimentally reproduce the real slipper dynamics within the pump and a certain degree of approximation must always be accepted during tests. The state of the art for the experimental investigation of the slipper-swash plate coupling in axial piston pumps is set by [5], where a redesigned three-piston pump is used as a test rig to minimize the alterations to the original component while still ensuring the required space for the sensors. A significant step towards a deeper knowledge of the slipper interaction with the other components of the pump was achieved with the development of modern

E-mail address: Francesco.orlandi@unimore.it (F. Orlandi).

https://doi.org/10.1016/j.ijft.2024.100992

Available online 29 November 2024

Nomenclature

B_G	Slipper balance coefficient
c	Speed of sound for mineral oil [m/s]
CAD	Computer Aided Design
CFD	Computational Fluid Dynamics
CPU	Central Processing Unit
DFBI	Dynamic Fluid Body Interaction
FEM	Finite Element Method
F_{Gab}	Lift force [*N*]
F_{NS}	Load pressing force [*N*]
$F_{pi,i}$	Pressure force acting on the piston surface area [*bar*]
$F_{pi,\mathrm{i-sl,\,i}}$	Effective force exerted by piston on the slipper [*bar*]
$F_{pi,\max}$	Maximum pressure force acting on the piston surface area at full pump displacement [*bar*]
h_0	Nominal gap height [*m*]
d	Slipper and Swash Plate minimum distance [*m*]
p	Pressure [*bar*]
Q_{LEAK}	Leakage flow [kg/s]
Q_{MAX}	Maximum pump flow rate [kg/s]
β	Swash plate tilt angle [°]
ρ	Density [kg/m^3]
ρ_0	Density at the atmospheric pressure [kg/m^3]
Ψ	Slipper tilt angle [°]
Ψ_{LIM}	Maximum slipper tilt angle from nominal gap conditions [°]

computers. Indeed, more and more detailed numerical models of the swash plate interface have been proposed by researchers. In [6], the CASPAR simulation tool was introduced for the first time. The possibility to simulate the entire piston machine including variable gaps and parts dynamics still make it one of the most advanced tools for the prediction of the viscous friction and gap flow losses. Along with the 0D-1D approach, several three-dimensional models have been developed to explain the occurrence of many localized phenomena which normally affect the pump performance as well as to quickly investigate the effects of possible geometrical, technological and physical solutions. In [7], a Finite Element Method (FEM) analysis highlights the stresses, strains, and forces associated with the crimping process in piston-slipper coupling, while a Computational Fluid Dynamics (CFD) methodology for the simulation of an entire swash plate type axial piston pump is described in [8]. In details, the model shows the effects of non-idealities on both pressure and force signals against theoretical results. A similar approach based on the Overset Mesh technique is adopted in [9,10], where the heat transfer between moving metal parts and oil in a piston pump and the influence of eco-friendly fluids on the performance of an external gear pump are studied, respectively.

In [11], the general flow and pressure drop equations of a real slipper architecture with single balancing groove are determined, and a comparison with the single land design is performed. A similar study is presented in [12], where different slipper geometries are compared in terms of pressure distribution, flow losses, and lift forces. In details, the variation of the hydrodynamic lift as a function of the groove position and length is discussed, and stationary CFD simulations are included to assess the pressure distribution within the clearance. However, a simplified approach based on fixed slipper positions is implemented in the code, therefore neglecting the dynamic effect of pressure forces on the slipper orientation. This paper aims at investigating the effects of a complete pump displacement variation on the instantaneous slippers dynamics in terms of motions, hydrodynamic balancing, leakages, and pressure distribution at the swash plate interface. In this regard, a previously presented CFD methodology, [13], based on a combined DFBI and morphing technique will be exploited to address the variable slipper position and clearance height under transient operating conditions. All theory and physic background is referred to as reported in the previous work of the authors [13], and will not be reproposed here.

2. Materials and methods

The proposed simulation was performed through the multi-purpose STAR-CCM+ v.2021.1.1 software, licensed by Siemens [14]. This work considered an industrial swash plate type axial nine-piston pump for closed loop applications with maximum continuous operating pressure of 420 bar and a rotational speed between 500 rev/min and 3800 rev/min. However, according to the datasheet of the component, the pump tolerates peak values of 450 bar and 4000 rev/min for very short periods of time. The internal CAD tools of the software were exploited to derive the fluid domain associated with a single slipper, and a circular sector of 40 degrees, i.e., 360 degrees divided by nine pistons, with a central mold of the slipper was obtained as a reference geometry for the simulation. Different fluid regions were further defined according to the principle of modularity, thus ensuring high controllability on both mesh quality and total number of cells. Moreover, an initial clearance height h_0 was set as a mean value of practical measurements performed on different samples of the same assembly. This has been measured with the machine turned off and with its components freshly new. This way a nominal value is taken into account to work as the reference initial clearance starting by ideal and not already worn out components (that would be impossible to take into account). A high-quality discretization of the 3D computational domain was reached to cope with the continuous mesh distortion caused by several slipper dynamics. An automated

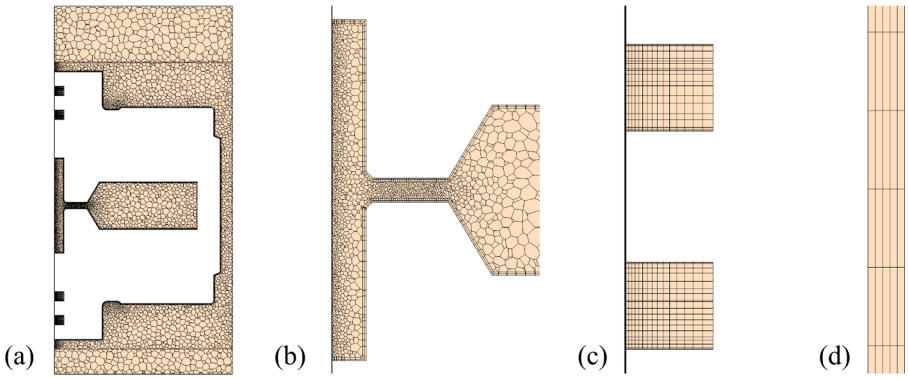

Fig. 1. Fluid domain discretization: (a) Mesh section of the entire fluid, (b) Slipper central, (c) Grooves, (d) Clearance

Table 1
Simulated operating conditions

Parameter	Symbol	Value
Rotational speed	n_{pump}	2500 rpm
Swash plate tilt angle	β	0-18 degrees
Supply pressure	p_{supply}	380 bar
Suction pressure	$p_{suction}$	20 bar
Drain pressure	p_{drain}	0.5 bar

polyhedral mesh was chosen to ensure a balanced solution with fewer cells than a tetrahedral mesh, [14], and local surface refinements were set at the wall boundaries of the slipper for an accurate prediction of the near-wall fluid-dynamic phenomena. Advanced meshing techniques were further exploited to address the flow through the thin slipper-swash plate gap and inside grooves. In details, a directed mesh approach was employed to provide a structured mesh in the axial direction, where five and fifteen layers of cells were respectively defined. Moreover, a butterfly mesh, [15], was manually sketched on the plane surface of the clearance region to achieve the highest possible degree of control on the volume mesh inside the gap. The final grid resulted in almost 3.4 million cells and 20 days were needed for the simulation of an entire shaft revolution on a modern cluster architecture of 160 CPUs. Please note that the implemented mesh is the minimum required in order to avoid the formation of negative volume cells in the clearance. In Fig 1a, a section view of the entire mesh is represented, while separate details of the slipper central pocket, the grooves, and the clearance are reported in Fig 1b – d, respectively.

A validated 0D-1D model of the entire pump was used to derive the input data for the proposed CFD model, and a real off-highway vehicles application was considered. An overview of the operating conditions is reported in Table 1.

In Fig 2, the pressure signal within the piston chamber is monitored over a complete swash plate stroke, i.e., from null to maximum tilt angle, and an initial settling was observed during the first three revolutions of the driving shaft. Subsequently, a periodic trend was repeated, till the maximum displacement was reached after fifteen shaft revolutions. Similar considerations were deduced from the evolution of the net piston force pressing the slipper towards the swash plate, $F_{pi,i\ -\ sl,\ i}$, which far represents the main contribution to the slipper motion, as reported by [13].

However, as reported in Fig 3 for the Piston-slipper force monitored during the same working cycle as in Fig 2, a progressive increment of the force during both suction and delivery intervals right after the initial transient is denoted. This suggests a non-periodic swash plate perpendicular force under constant pressure operations.

This concept is better explained by (1), where $F_{pi,i\ -\ sl,\ i}$ clearly increases with the swash plate inclination angle β, being $F_{pi,i}$ the pressure force acting on the piston effective area.

$$F_{pi.i-sl.i} = \frac{F_{pi.i}}{cos\beta} \tag{1}$$

Therefore, due to the extremely large computation time associated with a complete displacement variation, i.e., almost 300 days for the simulation of fifteen shaft revolutions, the proposed analysis was limited to the comparison between the initial transient and the maximum displacement operation, where the highest piston force acts on the slipper under stationary pressure conditions. Moreover, both the centrifugal force and the constraint with the retaining ring were included in the model by means of user-defined tables and field functions, while the separate contributions of inertia, weight and viscous friction were predicted by simulation. The three-dimensional nature of the forces was further addressed through local coordinate systems centred with the

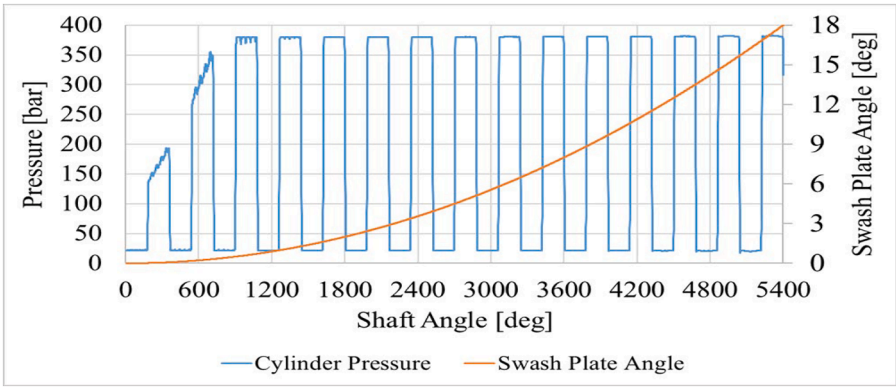

Fig. 2. Cylinder pressure and swash plate angle evolution during a complete pump displacement variation

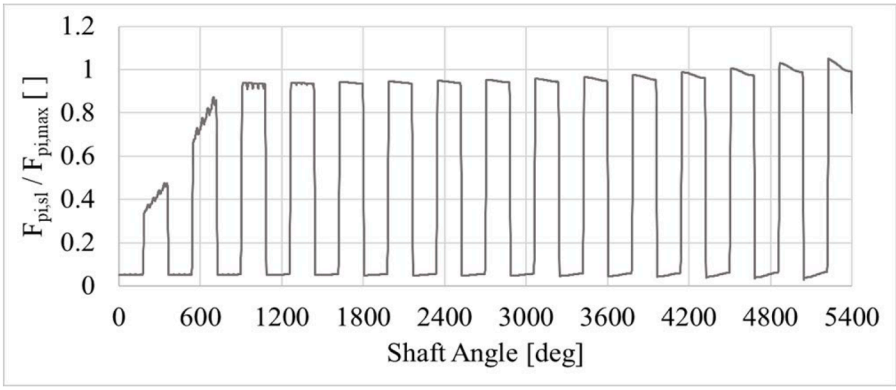

Fig. 3. Piston-slipper force

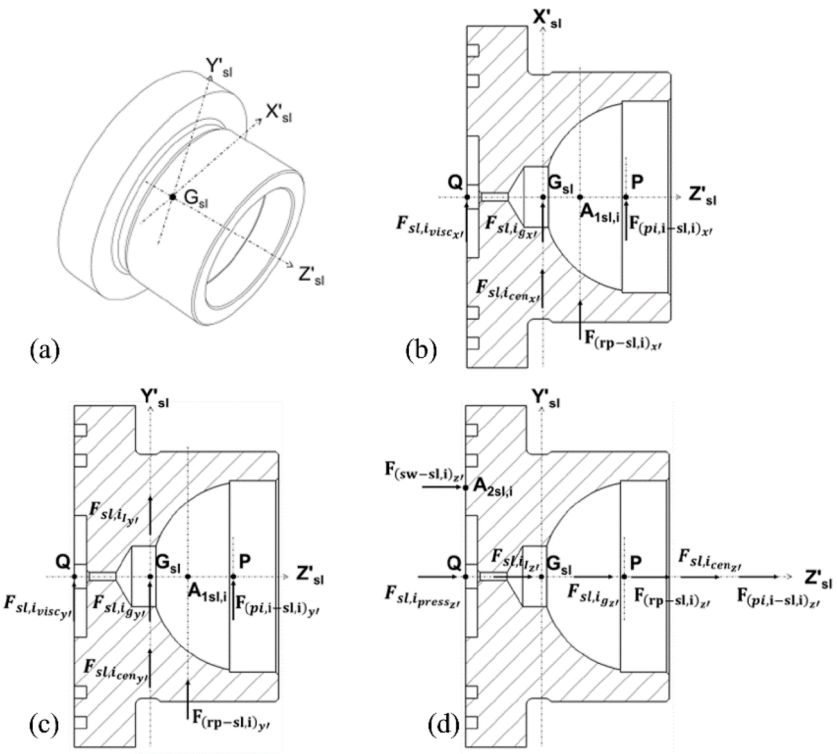

Fig. 4. Slipper free body diagram: (a) Slipper barycentric reference system, (b) X-forces, (c) Y-forces, (d) Z-forces

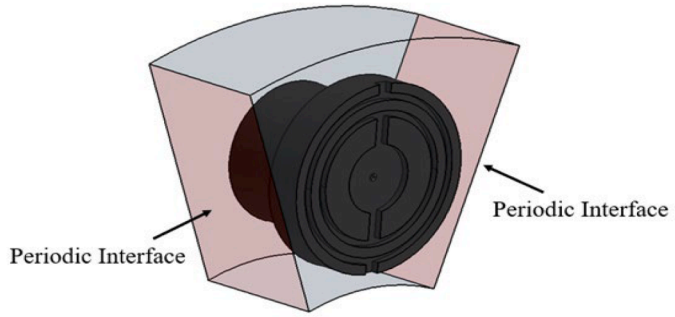

Fig. 5. Periodic interfaces

application points, qualitatively described in the free-body diagram of Fig 4.

The Dynamic Fluid Body Interaction (DFBI) algorithm was adopted to solve the governing equations of motion, therefore deriving the instantaneous slipper position in response to the external forces and moments. The axial translation as well as the tilting rotations were associated with the moving solid, while no spinning was considered for the proposed high-pressure application, as a result of [16]. In other terms, the slipper was modelled as a 3-DOF (Degrees of Freedom) rigid body with the simultaneous possibility to translate along the Z'_{sl} and to rotate about the X'_{sl} and Y'_{sl} axes, and a constant tangential velocity was set at the wall boundaries to mimic the effect of rotation about the shaft axis. Moreover, a periodic boundary interface of 40 degrees was defined at both sides of the fluid domain to account for the influence of the adjacent slippers, Fig 5. Indeed, the periodic interface can be used is CFD to cyclically repeat the information across two physically separated boundaries, so that the fluxes crossing one boundary are transformed and applied to the other through constant rotation or translation.

The morphing technique was combined with the DFBI model to cope with the mesh deformation produced by the slipper dynamics. Starting from a high-quality volume mesh, this specific tool of the software allows shifting the grid vertices according to the motion of boundaries and regions in transient analysis. However, the real contact between mating surfaces is not supported by the morpher, as it would produce zero or even negative volume cells in the mesh. Logically, this modelling limitation conflicts with the slipper design procedure presented in [1], which accepts a certain imbalance of the forces in favour of the piston pressing contribution with respect to the hydrodynamic lift since it is not desirable for the slipper to actually lift from the swash plate. For this reason, the contact coupling model was activated in the simulation to ensure a minimum clearance height between the parts, therefore preventing the slipper and the swash plate from colliding. In details, a return elastic force starts acting on the slipper along the swash plate normal axis as soon as the distance between the sliding surfaces drops below a user-defined effective range of $0.33h_0$, selected as the minimum setting to avoid mesh instability problems. With lower values of $0.33h_0$ the mesh generation would create negative cells leading to instability issues on the numerical calculations. This way, the chosen value acts as a minimum limit. The fluid compressibility was included in the simulation according to [10], and the actual properties of an ISO VG 32 mineral oil at the operating temperature of 80°C were set in the continuum panel. In (2), the physical variation of density as a function of the pump working pressure is described.

$$\rho = \rho_0 + \frac{p}{c^2} \tag{2}$$

A variable time step approach was implemented to reach the numerical stability of the solution under transient operating conditions. Quantitatively, a temporal discretization of 4 μs was used during suction, while a significant time step reduction was performed during both transitions and delivery intervals, where an incremental change of 1.33 μs proved necessary to put up with the strong pressure gradients and the extremely high working pressure. The K-ω SST turbulence model with the all-y+ wall treatment was chosen to precisely address the flow near the slipper surfaces for a better prediction of the hydraulic forces and torques. In addition, the Gamma Transition model was activated to assess the onset of transition in the turbulent boundary layer in terms of

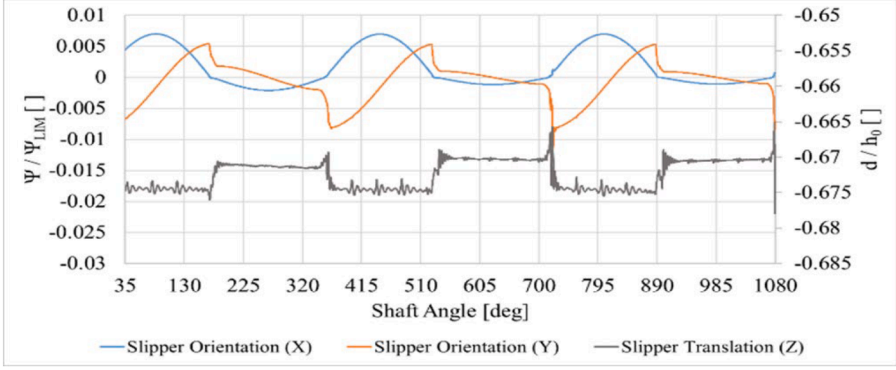

Fig. 6. Low pump displacement

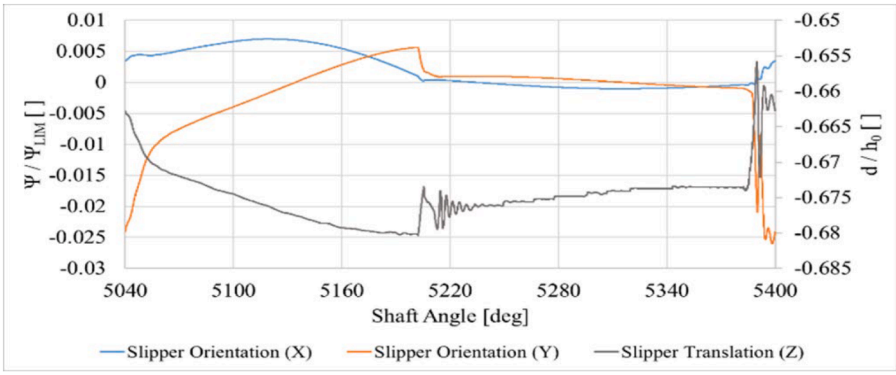

Fig. 7. Maximum pump displacement

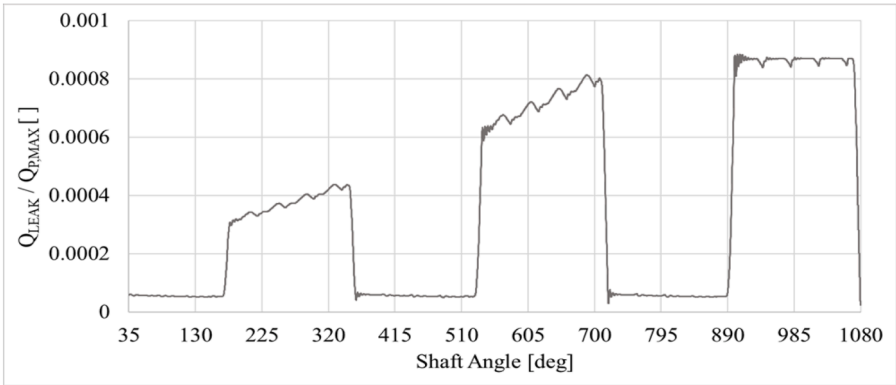

Fig. 8. Flow losses in low pump displacement

turbulence intermittency.

3. Results and discussion

In this chapter, the influence of the swash plate inclination angle on the slipper dynamics is investigated through a detailed comparison between the numerical results in the range of low displacement, i.e., during the first three shaft revolutions, and at maximum displacement. Please note that all the results were clipped at the shaft angle of 35 degrees to discard the non-physical solution associated with the initial solver stabilization. In Fig 6, both the slipper translation and orientation are reported on the same plot in the normalized form. At first, the sinusoidal curves highlighted a dominant tilting motion of the slipper during suction, while an almost null tilt angle suggested a uniform clearance height in the region of high-pressure. Moreover, an increment of the tilting amplitude was observed at maximum displacement in Fig 7. On the other hand, the translation term denoted a progressive reduction of the slipper-swash plate mean distance during suction, while a gradual lift was experienced along the delivery stroke of the piston. Furthermore, a slightly higher clearance compression was found with the increasing pump displacement, until a minimum gap height was reached at the transition from suction to supply under maximum displacement operations, in correspondence with the highest net piston force.

In Fig 8–9, the ratio of the flow losses to the ideal pump flow rate at the constant working speed of 2500 rev/min is reported. The results pointed out a proportional trend of the leakage with respect to pressure, while no obvious dependence on the machine displacement was noted after the initial pressure stabilization. In other terms, a major effect of the slipper-swash plate interface on the volumetric efficiency of the pump was observed at the delivery port opening due to the higher

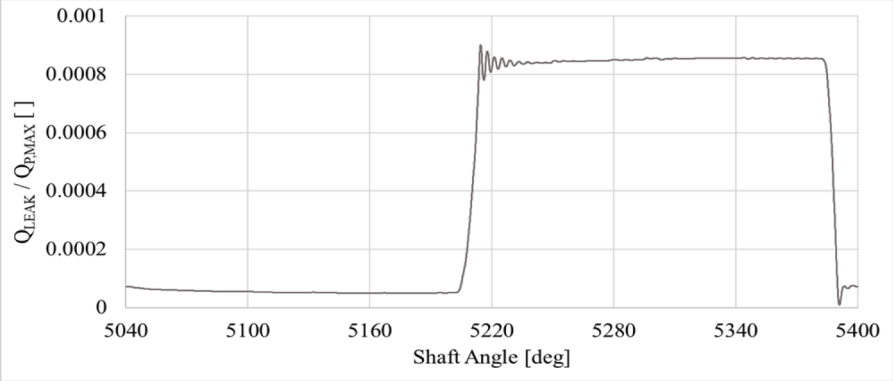

Fig. 9. Flow losses in maximum pump displacement

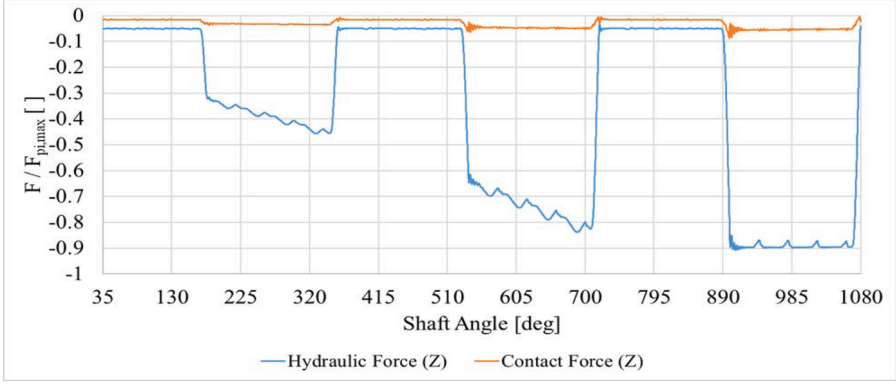

Fig. 10. Hydraulic and contact forces in low pump displacement

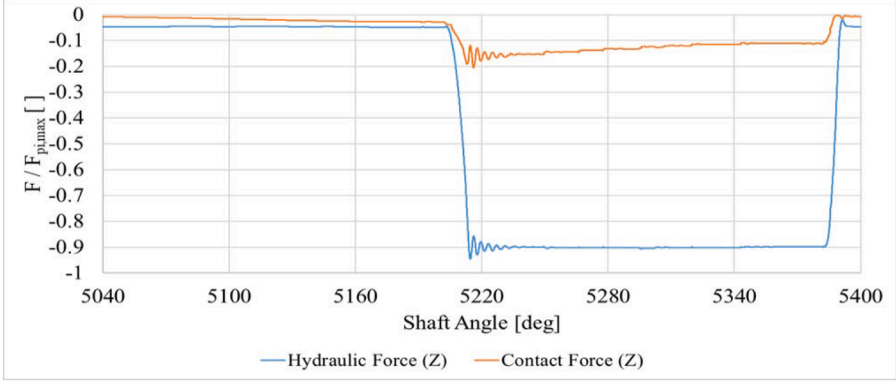

Fig. 11. Hydraulic and contact forces in maximum pump displacement

pressure drop across the gap.

Similar considerations were derived for the hydraulic force supporting the slipper on the swash plate. In Fig 10–11, the evident correlation with pressure outlined a dominant contribution of the hydrostatic component, thus leading to a higher force in the interval of fluid compression. In parallel, a close comparison with the DFBI contact force was added to the plot. The curves highlighted a considerable increment of the contact force with the swash plate inclination angle, while a negligible variation of the lift force was measured.

According to [1], the balance of forces acting on the slipper is normally expressed as a coefficient B_G defined as in (3), where F_{Gab} symbolizes the force trying to move the slipper away from the swash plate, while F_{NS} is the load pressing force.

$$F_{Gab} = B_G \cdot F_{NS} \tag{3}$$

As previously mentioned, a balance coefficient B_G lower than one represents the normal choice among the manufacturers to protect the volumetric efficiency of the pump, and a slight contact between the parts is accepted. In Fig 12–13, the balance coefficient is monitored on a full swash angle cycle, showing an almost perfect equilibrium of the forces, i.e., B_G between 0.9 and 1, in the intervals of high pressure. On the other hand, a more pronounced gap compression was expected during suction due to the higher discrepancy between the net piston force and the hydraulic lift. Moreover, an almost stationary condition, i.e., B_G equal to 0.75, was found in the range of low displacement, while a progressive reduction of the balance coefficient during maximum displacement operations led to an absolute minimum, i.e., B_G equal to 0.57, in the

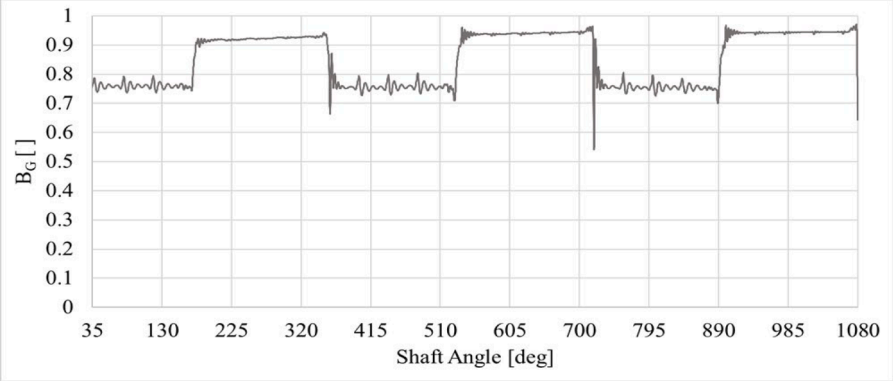

Fig. 12. Slipper balance coefficient for low pump displacement

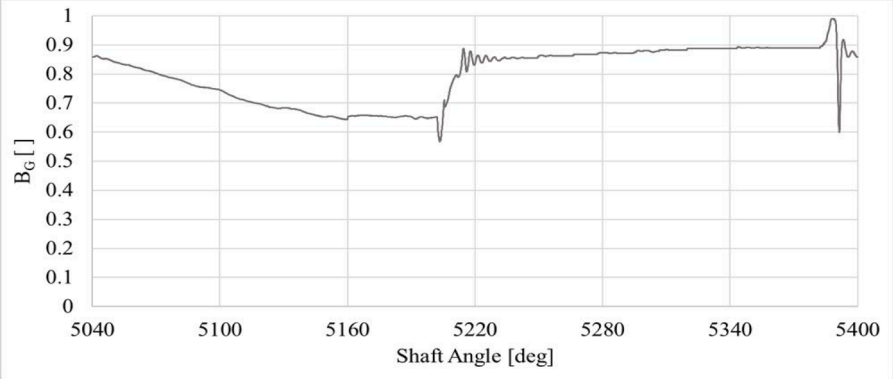

Fig. 13. Slipper balance coefficient for maximum pump displacement

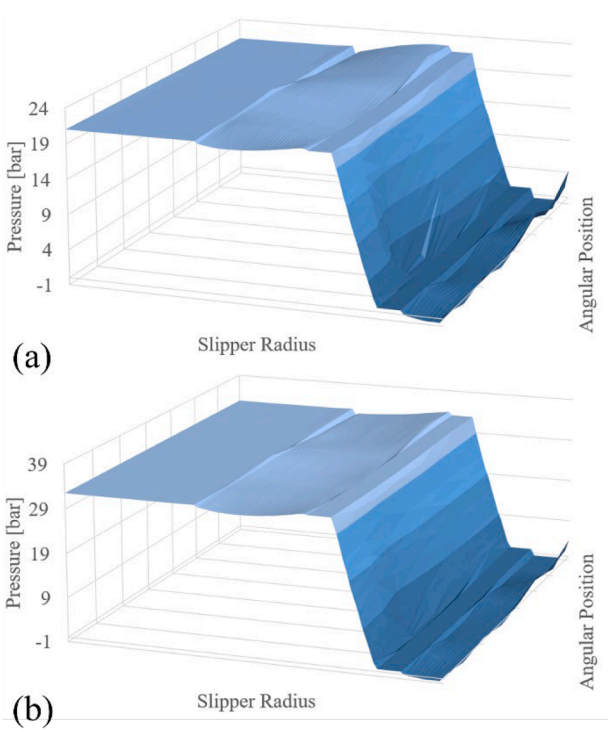

Fig. 14. Pressure distribution below the slipper sliding surface at maximum pump displacement (a) during suction (b) during supply

transition from suction to supply. Similar considerations were derived for the delivery stroke, where the non-compensated increment of the pressing force at maximum swash plate tilt angle produced a relevant reduction of the slipper balance coefficient, i.e., B_G below 0.9. In this phase, a linear increment of the coefficient with the piston stroke was observed, and a local peak, i.e., B_G almost equal to 1, was reached at the suction port opening. To summarize, these results denoted an important correlation between the pump displacement and the slipper dynamics. In details, a more rapid wear of the component is expected during high displacement and low-pressure operations due to the larger force unbalance, which could frequently lead to heavy collisions with the swash plate.

Finally, the pressure distribution within the clearance region was investigated by means of a structured grid of probes regularly arranged on the slipper sliding surface. In Fig 14, a three-dimensional representation of the pressure field at the interface with the swash plate during suction operations highlights a non-uniform pressure drop through the variable gap height due to the dominant slipper tilting. Conversely, Fig 14 shows a linear pressure drop between the inner and outer groove (identifiable with means of (a) in Fig 1 following the internal profile lines), in the interval of high working pressure, where the tilt cancellation leads to a uniform clearance height below the surface of the slipper. Moreover, a null value of the intermittency confirmed the fully laminar nature of the flow through the gap, [1].

4. Conclusion

This paper considered the effects of a complete displacement variation on the tribological elements of the slipper-swash plate interface in axial piston machines. A previously presented CFD methodology was exploited to simulate the dynamic fluid-body interaction of the slipper

under actual operating conditions. At first, a strict connection between the slipper dynamics and the working pressure of the pump was found. In details, a dominant slipper tilting was observed during suction, while a uniform clearance height was measured in the region of high working pressure, which denoted a parallel arrangement of the slipper with respect to the swash plate. Moreover, an evident correlation with the pressure distribution through the gap was derived. Actually, a homogeneous pressure drop was associated with a uniform clearance height, while local alterations were induced by variable height conditions. In terms of forces, the main contribution of the hydrostatic term on the slipper lift was demonstrated, with no obvious dependence on the pump displacement. On the other hand, a proportional increment of the contact force with the swash plate tilt angle was needed to cope with the incremental pressing force of the piston. According to (3), these results were further included in the analysis of the slipper design coefficient B_G. Indeed, a higher force discrepancy was achieved during suction operations due to the lower hydrostatic lift, and a progressive reduction of the balance coefficient with the increasing pump displacement was predicted. In other terms, those specific applications with maximum pump displacement, i.e., maximum flow rate, and low working pressure represent the most critical scenario for a proper lubrication of the slipper. To summarize, this manuscript points out all the inaccuracies related to the common assumption of a constant B_G between 0.95 and 0.99 in the design stage of axial piston pumps and motors, [1]. To conclude, the flow losses through the gap increased with pressure, while no apparent connection with the displacement was obtained. An accurate prediction of the multi-phase flow physics at the slipper-swash plate interface, such as the occurrence of both aeration and cavitation phenomena, would further enhance the results of the proposed simulation.

CRediT authorship contribution statement

G. Muzzioli: Writing – original draft, Software, Methodology, Data curation, Conceptualization. **F. Orlandi:** Writing – review & editing. **M. Venturelli:** Visualization, Supervision. **M. Milani:** Visualization, Supervision. **L. Montorsi:** Visualization, Validation, Supervision.

Declaration of competing interest

The authors declare that they have no known competing financial interests or personal relationships that could have appeared to influence the work reported in this paper.

Data availability

The data that has been used is confidential.

References

[1] Jaroslav Ivantysyn, Monika. Ivantysynova, Hydrostatic Pumps and Motors, Tech Books International, New Delhi, 2003.
[2] Hai J. Jiang, Bo Z. Wang, Long K. Wang, Power loss of slipper/swashplate based on elastohydrodynamic lubrication model in axial piston pump, in: IOP Conference Series: Earth and Environmental Science 188, 2018, https://doi.org/10.1088/1755-1315/188/1/012025.
[3] Gaston Haidak, Dongyun Wang, E. Shiju, Jun Liu, Study of the influence of slipper parameters on the power efficiency of axial piston pumps, Adv. Mech. Eng. 10 (9) (2018) 1–13, https://doi.org/10.1177/1687814018801460.
[4] Erdem Koç, Christopher J. Hooke, Considerations in the design of partially hydrostatic slipper bearings, Tribol. Int. 30 (11) (1997) 815–823, https://doi.org/10.1016/S0301-679X(97)00064-9.
[5] Junhui Zhang, Qun Chao, Bing Xu, Min Pan, Qiannan Wang, Yuan Chen, Novel three-piston pump design for a slipper test rig, Appl. Math. Model. 52 (6) (2017) 65–81, https://doi.org/10.1016/j.apm.2017.07.013.
[6] Uwe Wieczorek, Monika. Ivantysynova, Computer aided optimization of bearing and sealing gaps in hydrostatic machines – the simulation tool CASPAR, Int. J. Fluid Power 3 (1) (2002) 7–20, https://doi.org/10.1080/14399776.2002.10781124.
[7] Lawrence Y. Yao, Abir Z. Qamhiyah, Daniel X Fang, Finite element analysis of the crimping process of the piston-slipper component in hydraulic pumps, J. Mech. Des. 122 (3) (2000) 337–342, https://doi.org/10.1115/1.1286188.
[8] Massimo Milani, Luca Montorsi, Gabriele Muzzioli, Andrea Lucchi, A CFD approach for the simulation of an entire swash-plate axial piston pump under dynamic operating conditions, in: Proceedings of the ASME 2020 International Mechanical Engineering Congress and Exposition. Volume 10: Fluids Engineering, 2020, https://doi.org/10.1115/IMECE2020-23720. IMECE2020-23720 Virtual, Online, November 16–19.
[9] Massimo Milani, Luca Montorsi, Matteo Venturelli, A combined numerical approach for the thermal analysis of a piston water pump, Int. J. Thermofluids. 7-8 (2020), https://doi.org/10.1016/j.ijft.2020.100050.
[10] Gabriele Muzzioli, Luca Montorsi, Andrea Polito, Andrea Lucchi, Alessandro Sassi, Massimo Milani, About the influence of eco-friendly fluids on the performance of an external gear pump, Energies. (Basel) 14 (4) (2021) 799–827, https://doi.org/10.3390/en14040799.
[11] Josep M. Bergada, John. Watton, Axial piston pump slipper balance with multiple lands, in: Proceedings of the ASME 2002 International Mechanical Engineering Congress and Exposition, New Orleans, LA, 2002, https://doi.org/10.1115/IMECE2002-39338. IMECE2002-39338November 17–22.
[12] Josep M. Bergada, John. Watton, Force and flow through hydrostatic slippers with groove, in: Proceedings of the International Symposium on Fluid Control, Measurement and Visualization, Chengdu, China, 2005, https://doi.org/10.1115/IMECE2002-39338. August 22–25.
[13] Gabriele Muzzioli, Fabrizio Paltrinieri, Luca Montorsi, Massimo Milani, A CFD methodology for the analysis of the slipper-swash plate dynamic interaction in axial piston pumps, in: Proceedings of the 2022 IEEE Global Fluid Power Society PhD Symposium, Napoli, Italy, 2022. GFPS2022-1570819081October 12–14.
[14] Siemens PLM Software, "Star-CCM+ 2021.1.1 User Guide." Plano, TX, 2021.
[15] Valente Hernandez Perez, Mukhtar Abdulkadir, Barry J. Azzopardi, Grid generation issues in the CFD modelling of two-phase flow in a pipe, J. Comput. Multiph. Flows. 3 (1) (2011) 13–26, https://doi.org/10.1260/1757-482X.3.1.13.
[16] Thomas Ransegnola, Lizhi Shang, Andrea. Vacca, A study of piston and slipper spin in swashplate type axial piston machines, Tribol. Int. 167 (2022) 107420, https://doi.org/10.1016/j.triboint.2021.107420.